

## CONVENTIONAL AND SENSITIZED-RANS MODELING OF CONCENTRIC ANNULAR COUETTE FLOW

Xiaoyu Wang, Jeanette Hussong, Suad Jakirlić

Institute of Fluid Mechanics and Aerodynamics, Technical University of Darmstadt  
 Peter-Grünberg-Str. 10 64287 Darmstadt, Germany  
 jakirlic@sla.tu-darmstadt.de

### ABSTRACT

The turbulent Couette flow in a concentric annulus with rotating outer wall is computationally studied in a range of rotational intensities up to those that induce flow laminarization. The computational framework focuses on a comparative evaluation of two modeling approaches that consider the dynamics of the turbulent stress tensor  $\overline{u'_i u'_j}$  with a differential near-wall Reynolds Stress Model (RSM) as the underlying closure model. While this quantity refers to the turbulence modeled in its entirety within the conventional RANS (Reynolds-Averaged-Navier-Stokes) model scheme (Jakirlić & Hanjalić (2002)), its eddy-resolved version allows for the capture of fluctuating turbulence (Jakirlić & Maduta (2015)). In the context of the latter, scale-adaptive model formulation, the quantity is related only to the unresolved sub-scale turbulence. The scale-resolving capability of this Sensitized-RANS modeling strategy, employed within a time-accurate simulation, is enabled by the introduction of a production term into the scale-supplying equation, formulated in terms of the second derivative of the underlying velocity field, in accordance with the SAS (Scale-adaptive Simulation) proposal of Menter & Egorov (2010). The results obtained by the Sensitized RANS-RSM exhibit a high degree of agreement with the LES reference by Hadžiabdić *et al.* (2013) with respect to the mean velocity and turbulence fields as well as the vortex characterization in terms of eddy shape and size as a function of rotational intensity increase. This is manifested by the enhancement of the stabilizing effect on the turbulence activity, modifying the vortical structures appropriately toward their differently intensified alignment with the flow directional orientation.

### INTRODUCTION

The flow configurations resembling annular flow between two cylinders, cylindrically or eccentrically arranged, are of great practical - such geometries are found, for example, in journal bearings, heat exchangers, and mixers - and scientific importance. Accordingly, a considerable amount of work has been done, for example, on flow in a swirl burner (Hübner *et al.* (2003)), electroconvective flows (Huang *et al.* (2023)), wall heating (Bagheri & Wang (2021)), and non-Newtonian fluid flows (Nouri & Whitelaw (1997)) in such geometries, as well as on concentric annular flow with counter-rotating and co-rotating walls. The latter configurations correspond to the general situation of a Taylor-Couette flow system, Grossmann *et al.* (2016). According to the  $(Re_o, Re_i)$  phase diagram, which illustrates the variations of the flow regime as a function of the Reynolds numbers based on the rotating wall velocity (Andereck *et al.* (1986), Grossmann *et al.* (2016);

$Re_o = U_{\theta, wall}(R_o - R_i)/\nu$ ), the presently considered flow corresponds to a circular Couette flow with rotating outer wall and non-rotating inner wall ( $Re_i = 0$ ), Fig. 1; the rate of rotation is defined as  $N = U_{\theta, wall}/U_{bulk}$ . The corresponding reference database was provided by Hadžiabdić *et al.* (2013) who performed a Large-Eddy-Simulation using the dynamic Smagorinsky subgrid-scale model. The LES study covers the range of rotation rates  $N = 0.5, 1.0, 2.0, 2.8$  and  $N = 4$ , with the latter case undergoing a complete flow relaminarization.

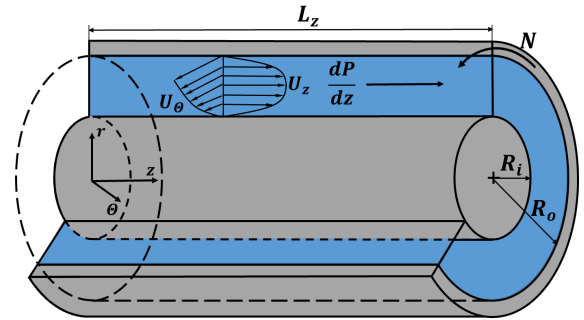


Figure 1: Schematic of the flow configuration considered

The present work analyzes the structural properties of the concentric annular Couette flow over the range of rotational intensities indicative of a turbulent regime in the context of a time-accurate Reynolds-Averaged Navier-Stokes (RANS) simulation, with an appropriately sensitized Reynolds stress model describing the dynamics of the unresolved subscale motion. This model, known as the Improved Instability-Sensitive Reynolds Stress Model (IISRSM), allows the use of the entire sub-scale Reynolds stress tensor, which makes it possible to account for the anisotropy of the residual turbulence. For the purpose of comparative assessment, the results of the conventional Reynolds Stress RANS Model are also evaluated. As it will be seen in the 'Results and Discussion' section, the application of the conventional RANS model leads to a premature flow laminarization of the flow already at the rotation rate  $N = 2.0$ , while the IISRSM returns turbulent flow structure in the entire  $N$ -range up to  $N = 2.8$ , closely following the reference LES.

### COMPUTATIONAL MODEL

The incompressible flow in a concentric annulus with outer wall rotation is governed by the following Reynolds-

Averaged Navier-Stokes Equations in an unsteady framework:

$$\frac{\partial}{\partial t}(\overline{U}_i) + \overline{U}_j \frac{\partial(\overline{U}_i)}{\partial x_j} = \frac{\partial}{\partial x_j} \left[ \nu \left( \frac{\partial \overline{U}_i}{\partial x_j} \right) - \overline{u'_i u'_j} \right] \quad (1)$$

The velocity  $\overline{U}_i$  represents the time-averaged field when solved by a conventional Reynolds Stress Model (RSM), or the instantaneous field in the context of the Sensitized-RANS method. Correspondingly, the stress tensor  $\overline{u'_i u'_j}$  is representative of the fully modeled turbulence in the framework of the former method, or only of the unresolved sub-scale turbulence when used in conjunction with the latter modeling scheme. In both cases, the dynamics of the stress tensor components  $\overline{u'_i u'_j}$  is described by a second-moment closure formulation by solving the following transport equation (Jakirlić & Hanjalić (2002)):

$$\frac{D\overline{u'_i u'_j}}{Dt} = P_{ij} + \Phi_{ij} - \varepsilon_{ij}^h + \frac{\partial}{\partial x_k} (0.5D_{ij}^v + D_{ij}^t) \quad (2)$$

The source terms on the RHS of the Reynolds stress transport equation describe the exactly treated production rate  $P_{ij}$ , the redistribution process  $\Phi_{ij}$ , the viscous dissipation correlation  $\varepsilon_{ij}$ , and viscous and turbulent diffusion transport  $D_{ij}^{(v+t)}$ . The molecular diffusion  $D_{ij}^v$ , can be treated exactly, as well as the production rate  $P_{ij}$ ; all other processes have to be modeled adequately. In contrast to a conventional RANS Reynolds stress model, which is incapable of describing any spectral dynamics of the turbulence field, the present IIS-RSM, representing its scale-resolving version, is appropriately sensitized to adequately capture turbulent fluctuations. The latter feature is introduced according to the SAS (Scale-Adaptive Simulation) methodology proposed by Menter & Egorov (2010). The model accounts for an additional production term introduced into the specific dissipation rate equation of  $\omega^h = \varepsilon^h/k$ , with  $\varepsilon^h = \varepsilon - 0.5D_k^v$  and  $k = 0.5\overline{u'_i u'_i}$ , depending primarily on the second derivative of the underlying velocity field:

$$\frac{D\omega^h}{Dt} \Big|_{IISRSM} = \frac{D\omega^h}{Dt} \Big|_{RSM} + P_{IISRSM} : P_{IISRSM} = f \left( \frac{\partial^2 \overline{U}_i}{\partial x_j \partial x_j} \right) \quad (3)$$

A unique feature of the model is its ability to adapt to the scales present in the unresolved residual motion by interacting with the underlying grid resolution. This adaptive feature facilitates the development of turbulent fluctuations. Unlike the original SAS proposal, which relies on the von Karman length scale ( $L_{vK} \propto \nabla \overline{U}_i / \nabla^2 \overline{U}_i$ ) as the triggering parameter to activate the resolving mode, the current approach models this parameter solely in terms of the second velocity derivative. This modification is due to the integral length scale equation described in Rotta (1972) Rotta (1972). This adjustment makes the model more sensitive to turbulence fluctuations and allows the use of even coarser grid resolutions.

For the complete specification of the turbulence model and all related details regarding its numerical treatment, the interested reader is referred to Jakirlić & Maduta (2015) and Joksimović & Jakirlić (2023).

## CASE DESCRIPTION / NUMERICAL DETAILS

The flow configuration considered here is a concentric annulus with outer wall rotation, Fig. 1. The bulk Reynolds number of the axial flow is  $Re_b = U_{bulk} D_h / \nu = 12500$  ( $D_h = 2(R_o - R_i)$ ). The ratio of the outer radius to the inner radius, known as the curvature parameter, is  $R_i/R_o = 0.5$ . The rotating wall velocity based Reynolds numbers  $Re_o$  of 3125, 6250, 12500 and 17500 correspond to the presently considered rotation rates of  $N = 0.5, 1.0, 2.0$  and  $2.8$  respectively. In addition, the non-rotating annular flow was also computed. The length of the solution domain, taking into account the full circular cross sectional area, varied between  $10\delta$  and  $40\delta$  ( $2\delta = R_o - R_i$ ) depending on the rotation rate, with shorter lengths corresponding to lower rotation rates. The grid size applied for the IISRSM simulation varies between 1.8 million cells (for shorter lengths and lower rotation rates) and 7.4 million cells for  $N = 2.8$  and  $L_z = 40\delta$ .

All simulations are performed with the finite-volume based open source toolbox OpenFOAM® (Open Source Field Operation and Manipulation). While the conventional Reynolds stress model uses the steady-state RANS computations, its instability-sensitized version is applied in the time-accurate RANS framework with 2nd order accurate time integration. A controlled adaptive time step ensures a Courant number less than one throughout the solution domain. The discretization of the convective terms in the momentum equations is performed using the 2nd order accurate Central Differentiation Scheme (CDS). The flow domain is meshed using the OpenFOAM mesh utility called 'blockMesh'. The mesh is generated with an appropriate cell refinement grading toward the walls, such that the closest computational node to the wall is well inside the viscous sublayer and has a dimensionless wall distance  $y^+$  substantially less than one.

## RESULTS AND DISCUSSION

Fig. 2 shows the instantaneous axial velocity in all four rotating flow configurations considered, resulting in a turbulence field using the IISRSM, illustrating the shape and size diversity of vortical structures under the influence of increasing rotational intensity. The scale-resolving capability of the IISRSM is clearly visible at the velocity fields exhibiting turbulent fluctuations. The dynamics of the velocity field is mainly driven by the resolved turbulent velocity field entering the momentum equation via the convective term. Close to the wall, however, the modeled sub-scale turbulent stresses are dominant and therefore crucial for the correct capture of the near-wall streaks.

It is evident that in the near-wall region, the rotation-induced centrifugal effects elongate the eddy structures populated in the radial and azimuthal directions, which are responsible for the generation of turbulent shear stress. For  $N = 0.5$ , the elongated streaky structures are clearly aligned along the streamwise flow direction, implying a negligible effect of rotation. As the rotation intensity increases to  $N = 1$ , the streaks show discernible inclination in the region adjacent to the inner wall illustrating that the outer-wall rotation has perpetuated to the region very close to the non-rotating wall. In contrast, for  $N = 0.5$  the instantaneous field near the outer wall shows no distinct difference with that near the inner wall; the stripes at the outer wall of  $N = 1$  tend to be shorter and thicker; the distribution of these stripes becomes more irregular. This irregularity appears at the inner wall of  $N = 2$ , where the enhanced inclination of streaks is still noticeable. However, the typical wall-adjacent streaky pattern is barely visible at the outer wall

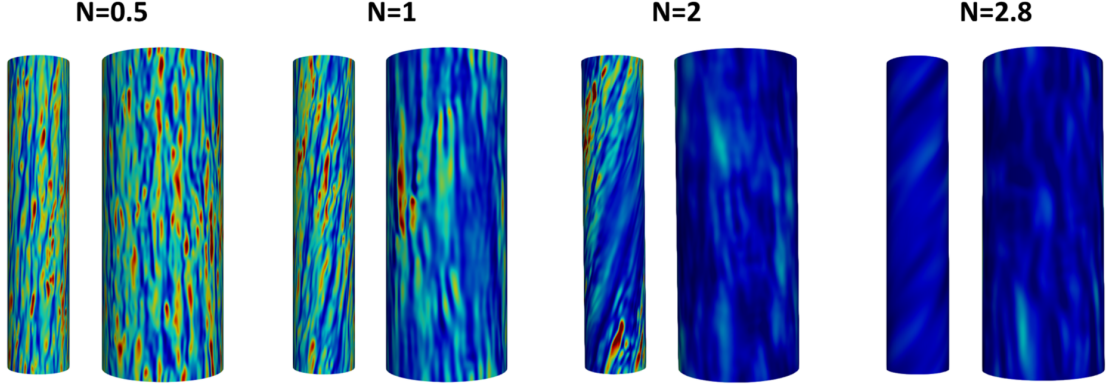


Figure 2: Instantaneous axial velocity field at inner (left images) and outer (right images) wall at distance corresponding to  $y^+ \approx 5$  over the full range of rotational intensities considered

Table 1: Mean flow parameters for the annular flow over the full range of rotational intensities

N	$Re_\tau(\text{Inner})$			$Re_\tau(\text{Outer})$			$C_f$		
	RANS	IIS	LES	RANS	IIS	LES	RANS	IIS	LES
0	210.00	212.81	209.38	199.69	193.75	184.38	0.008455	0.008217	0.007634
0.5	208.13	212.50	209.38	199.69	192.19	178.13	0.008115	0.008126	0.007325
1	198.75	202.81	203.13	181.25	171.25	156.25	0.007182	0.006812	0.006150
2	108.13	164.69	165.63	93.75	135.63	134.38	0.001998	0.004363	0.004338
2.8	105.63	115.94	118.75	92.81	127.81	125.00	0.001938	0.003148	0.003096

region, indicating that the large-scale turbulent structures are more dominant here. As the rotation is further intensified to  $N = 2.8$ , the streaks almost disappear in both the inner and outer wall regions, indicating that the turbulence fluctuations are gradually decreasing and the flow tends to be laminar.

Table 1 shows the main flow parameters for the annular Couette flow at different rotation rates within the framework of the present study, along with the reference LES data. Here the friction Reynolds number is based on the streamwise friction velocity  $u_{\tau,z}$ . The skin friction coefficients are calculated using the averaged friction velocity ( $C_f = \tau_z / \frac{1}{2} \rho U_b^2$ ). As the rotation rate  $N$  increases, the friction-based Reynolds number related to the inner wall shows a slight decrease up to  $N = 1$ , after which it experiences a significant reduction. Analogously, the Reynolds numbers derived from the friction velocity associated with the outer wall consistently decrease, with values lower than those in the inner wall region. This pattern suggests that the rotation of the outer wall exerts a stabilizing effect on the turbulence field, reflecting its lagging behavior with respect to the inner wall region, which is relevant for the energy transported by the cross-flow. It is noteworthy that the flow parameters obtained by the conventional RANS model show a significant decrease in accuracy at a rotation rate of  $N = 2$  and  $2.8$  compared to those obtained by IIS-RSM with respect to LES. This highlights the weak predictive performance of the conventional RANS model for cases with higher outer wall rotation rates. This limitation will be discussed in more detail below.

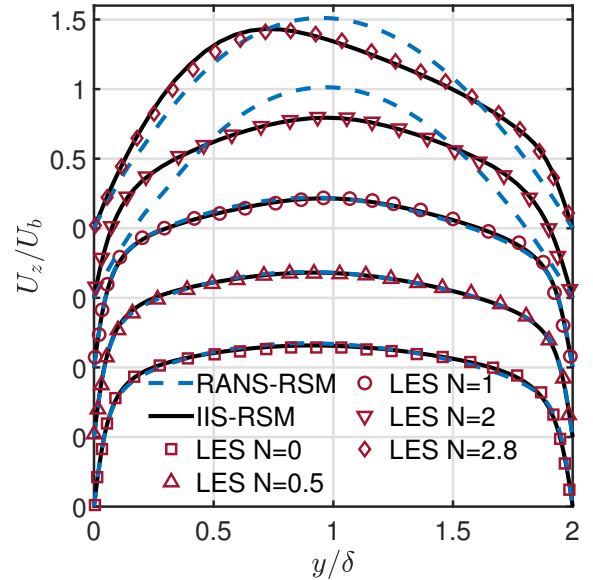


Figure 3: Profile development of the mean axial velocity in linear scaling over the full range of rotational intensities

Fig. 3 shows the mean streamwise velocity profile calculated with conventional RANS and IIS-RSM models in comparison with LES data from Hadžiabdić *et al.* (2013) for in-

creasing outer rotation rates. While the axial velocity distributions at low rotation rates  $N = 0.5$  and 1 show symmetric profiles with negligible deviation from that of the non-rotating case, the velocity profile at  $N = 2$  tends to be quasi-laminar and this development intensifies as the rotation rate increases further up to  $N = 2.8$ . The suppression of turbulence is indicated by the dramatic increase of the asymmetrically positioned profile maximum in the core region and the corresponding weakening of the velocity gradient near the walls. This laminarization tendency implies a strong turbulence damping within the flow configuration and thus poses a major challenge for the RANS approach to capture the associated turbulence flow properties Jakirlić *et al.* (2002). It is evident that despite the satisfactory agreement of the conventional RANS results with the LES data at the lower rotation rates  $N = 0, 0.5$  and 1, the axial velocity profile tends to become prematurely laminar at the higher rotation rates  $N = 2$  and 2.8. Nevertheless, the anomaly of the conventional RANS Reynolds stress model with respect to the premature relaminarization at increased rotation rates has been remedied by its eddy-resolving IIS-RSM version, where the velocity profiles show very good qualitative and quantitative agreement with the LES data.

The tendency of the velocity profile to establish a laminar-like shape can be further observed in Fig. 4, which shows the logarithmic plots of the effective, i.e. resultant velocity with respect to the inner non-rotating wall (upper) and the outer rotating wall (lower), taking into account both the streamwise and azimuthal velocity components; the modulus of the velocity vector  $|U| = \sqrt{U_z^2 + (U_w - U_\theta)^2}$  is normalized by the corresponding effective friction velocity ( $U_f = \sqrt{U_{f,z}^2 + U_{f,\theta}^2}$ ,  $U_{f,z} = \sqrt{v(\partial U_z / \partial r)_{wall}}$ ,  $U_{f,\theta} = \sqrt{v(\partial U_\theta / \partial r)_{wall}}$ ). While both RSM models provide reliable results for the non-rotating case as well as for the lower rotation rate cases  $N = 0.5$  and 1 with respect to the normalization by both the inner and outer wall shear stress parameters (cf. Table 1), the difference in the predictive capability in capturing the velocity profiles when approaching the laminar limit at higher rotation rates is evident. The application of the conventional RANS model results in a fully established laminar profile at both walls already for  $N = 2$  as well as for 2.8, which is consistent with the previous discussion regarding premature relaminarization. In contrast, the velocity profiles predicted by IIS-RSM show a correctly reproduced stabilizing rotational tendency, leading to a turbulent-laminar transition flow regime that closely follows the reference LES data in both magnitude and profile shape, with a significant overshoot compared to the logarithmic law of the wall.

The effect of rotation on the Reynolds stress components is shown in Fig. 5. For cases with no rotation and low rotation rates ( $N = 0.5$  and 1), the results obtained by both RSM formulations are in good qualitative and quantitative agreement with the LES data. In particular, the IIS-RSM demonstrates an advanced capability in capturing the asymmetric characteristics of the Reynolds stress components, which is especially evident for the radial normal stress component  $\overline{u'_r u'_r}$ , as depicted in Fig. 5 (b). Here, the conventional RANS model erroneously predicts a quasi-symmetric distribution across the annulus with nearly identical maxima in the inner and outer wall regions. However, it is noteworthy that the IIS-RSM slightly overpredicts the streamwise component  $\overline{u'_z u'_z}$  near the rotating wall (Fig. 5 (a)), where rotational effects begin to weakly stabilize the flow. A further increase of the rotation rate to  $N = 2$  and 2.8 intensifies the discrepancies in the prediction of the second-order statistics: the conventional RANS model is inca-

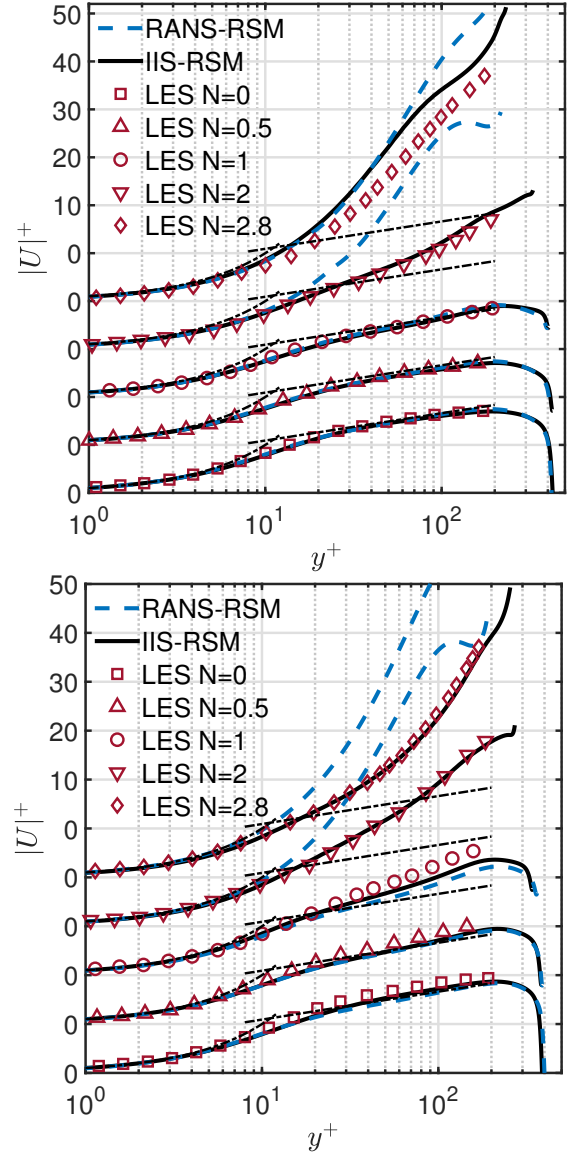


Figure 4: Semi-log plots of the resultant velocity (considering both axial and azimuthal components), with respect to the inner non-rotating wall (upper) and the outer rotating wall (lower), over the full range of rotational intensities

able to correctly predict the Reynolds stress field, resulting subsequently in the premature relaminarization with all stress components exhibiting zero values across entire flow domain, whereas the IIS-RSM delivers an increasingly asymmetrical Reynolds stress profile behavior and quantitatively accurate results, agreeing very well with the reference LES database. A minor deviation is observed in the IIS-RSM related predictions for the component  $\overline{u'_\theta u'_\theta}$  at the highest rotation rate of  $N = 2.8$ .

It is clearly seen that the increase of the rotation intensity causes a significant modification of the Reynolds stress components in the region close to the rotating wall, while the values close to the non-rotating wall remain largely unchanged up to  $N = 2$ , beyond which the flow structures are subjected to a significant modulation. Within the rotational intensity range including  $N = 2$ , an increasing asymmetry of all Reynolds stress component profiles is observed with a gradual decrease of their intensity in the region adjacent to the outer wall. In parallel, a slight but systematic increase of the Reynolds stress

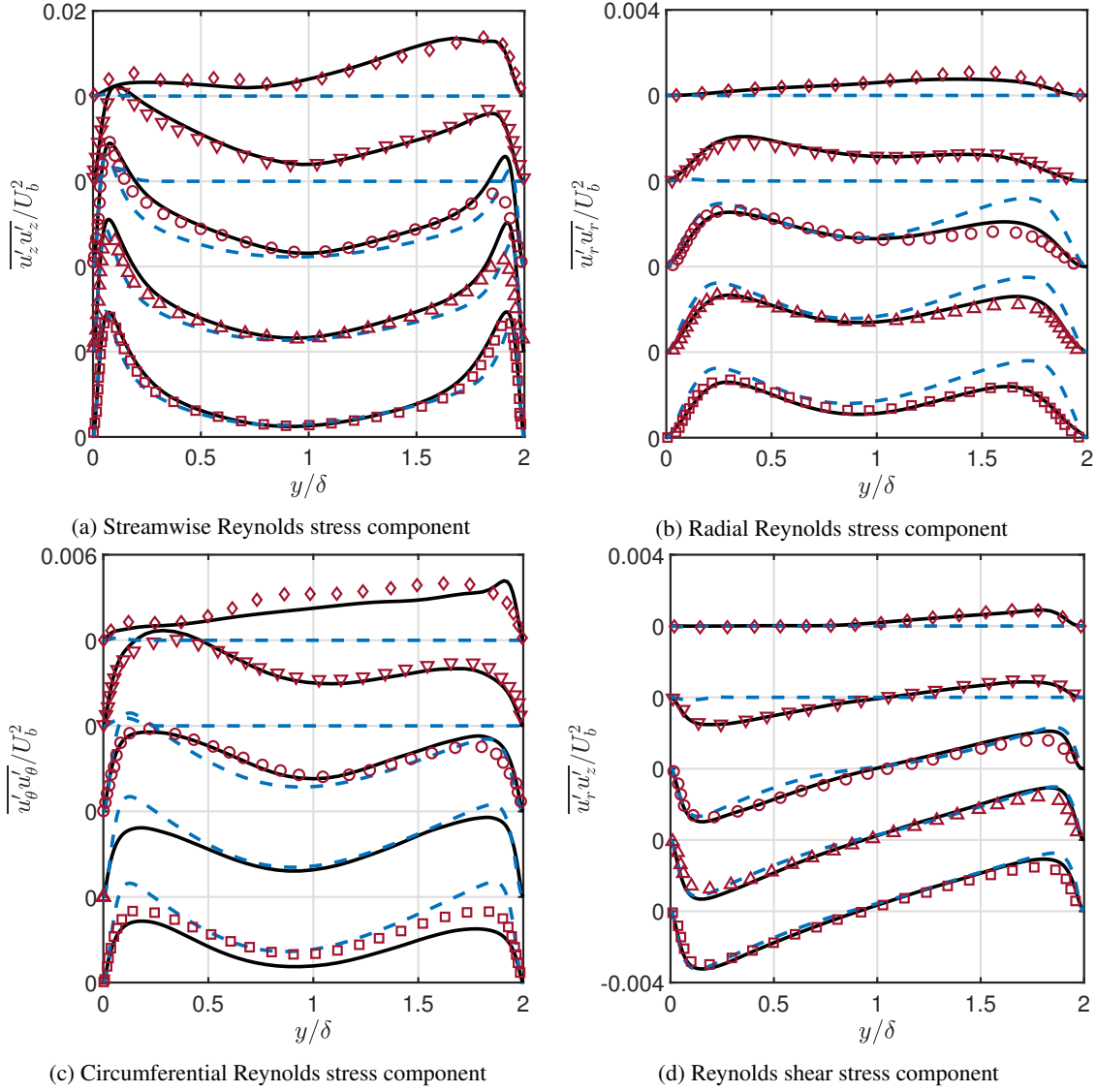


Figure 5: Profile development of the Reynolds stress components over the full range of rotational intensities

intensity components is observed in the vicinity of the inner non-rotating wall. Higher  $Re_\tau$  values, which are representative of the wall shear stress, compared to those evaluated at the outer wall clearly indicate a higher velocity gradient at the inner wall, which is a major source of turbulence production, cf. Table 1. However, at the highest rotational intensity of  $N = 2.8$ , whereas all diagonal Reynolds components approximately maintain their near-wall maxima at the outer wall region, their dramatic decrease, almost complete disappearance, is observed at the inner wall. This is also reflected in a significant reduction in wall shear stress at the inner wall compared to the outer wall, cf. Table 1. Similar effects can be observed on the profiles of the Reynolds shear stress component  $\overline{u_r'u_z'}$ . A pronounced, global decrease in turbulence intensity in the vicinity of the non-rotating cylinder wall implies that the stabilizing effect induced by the outer wall rotation permeates the entire annular gap.

The barycentric interpretation of the Reynolds stress anisotropy map for annular flow with different outer wall rotation rates is shown in Fig. 6, aiming to access the influence of the rotating outer wall on the turbulent anisotropy. In the barycentric map, the specific properties of turbulence anisotropy are intuitively illustrated by using a combination of realizable turbulence states, with the three map corners re-

ferring to their equally weighted limiting states according to Banerjee *et al.* (2007). The anisotropy trajectories for both the non-rotating inner wall and the rotating outer wall are initiated at the map boundary connecting the one-component  $X_{1C}$  and the two-component  $X_{2C}$  turbulent states. These wall points are shifted towards the two-component turbulence state by increasing the rotation intensity, which is consistent with the stabilizing effects on the turbulence structure, as observed for example in the axially rotating pipe flow subjected to increasing rotational intensity, as discussed in Jakirlić *et al.* (2002). The endpoint of the black colored trajectory located at half the distance between the inner and outer walls, which represents the non-rotating case in both plots, tends to approach the state of the so-called axisymmetric expansion limit, which is characterized by the weakest anisotropy level in the entire cross section, with values of Lumley's two-componentality parameter  $A \approx 0.8$ . Similarly, the end points of the anisotropic trajectories for the rotating flow cases denote accordingly the core flow locality with a weakest anisotropy level for the given rotational intensity. The corresponding  $A$  values for the lower rotation rates  $N = 0.5$  and  $1.0$  are  $0.7 - 0.8$  (the plot of the  $A$  profiles is not shown here for brevity). On the other hand, the anisotropy trajectories for the higher rotation rates considered,  $N = 2.0$  and  $2.8$ , show a much stronger anisotropy level, with

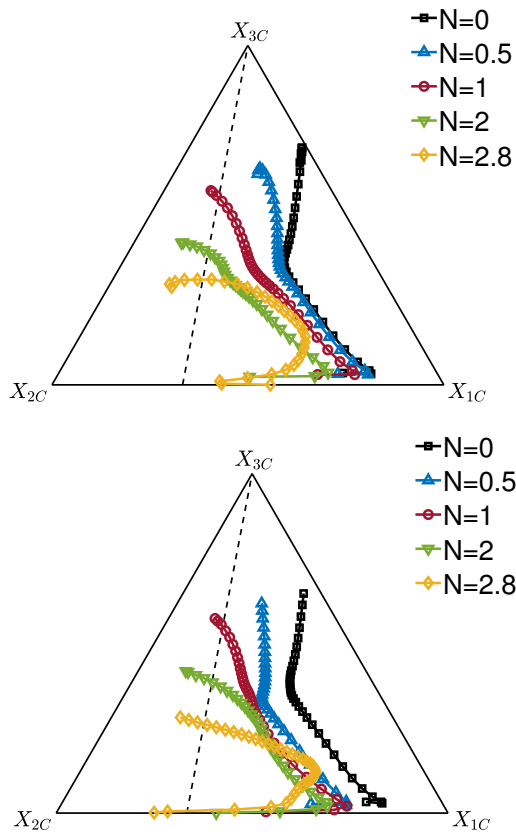


Figure 6: Barycentric interpretation of the Reynolds stress anisotropy with respect to the inner- (upper) and outer- (lower) wall region obtained by the Sensitized RANS-RSM over the full range of rotational intensities

the  $A$  value decreasing to  $\approx 0.5$ . The endpoints of the trajectories lie well within the anisotropy map, with a clear shift to the left of the map boundary indicating the axisymmetric contraction state of the turbulence, consistent with a global suppression of turbulence intensity as a function of rotation rate increase.

## CONCLUSION

In the present study, the conventional RANS model and its eddy resolving version IIS-RSM were used to simulate the fully developed turbulent flow in the concentric annulus at  $Re_{D_h} = 12500$  and curvature parameter  $R_i/R_o = 0.5$  with an axially rotating outer wall at different rotation rates up to  $N = 2.8$ . The capture of mean flow properties and second order statistics by conventional RSM shows good qualitative and mostly quantitative agreement with reference LES for lower rotation rates  $N = 0.0, 0.5$  and  $1.0$ , but shows premature relaminarization for higher rotation rates already at  $N = 2.0$  and  $2.8$ . In comparison, the flow properties provided by the eddy resolving IIS-RSM are more consistent with the LES reference data for all rotation intensities considered. The results indicate that the axial velocity profiles tend to deviate from the equilibrium conditions expressed by the law of the wall toward a laminar-like regime as  $N$  increases. On the other hand, the Reynolds stress intensities retain their turbulent content, with the pronounced suppressing tendency in the vicinity of the non-rotating wall for the highest rotation rate. Related to the inherent capability of the IIS-RSM to adequately resolve the turbulence fluctuations, the turbulence anisotropy was investigated using the barycentric map to

estimate the influence of the rotating outer wall on the characteristic turbulence states. The barycentric interpretation of the Reynolds stress anisotropy shows the tendency of the flow toward the two-component axisymmetric contraction state with a systematically enhanced anisotropy level in the core region with increasing  $N$ .

**Acknowledgment.** The authors gratefully acknowledge the German Federal Ministry of Education and Research (BMBF) and the federal state of Hessen for supporting this project as part of the NHR4CES (National High Performance Computing Center for Computational Engineering Sciences) funding at TU Darmstadt and RWTH Aachen and the Deutsche Forschungsgemeinschaft (DFG, German Research Foundation) in the framework of the Collaborative Research Center/Transregio 361 (CRC-TRR361, project ID 492661287). The authors furthermore acknowledge the computing time granted on the Lichtenberg HPC of the TU Darmstadt.

## REFERENCES

- Andereck, C.D., Liu, S.S. & Swinney, H.L. 1986 Flow regimes in a circular couette system with independently rotating cylinders. *Journal of Fluid Mechanics* **164**, 155–183.
- Bagheri, E. & Wang, B.-C. 2021 Direct numerical simulation of turbulent heat transfer in concentric annular pipe flows. *Physics of Fluids* **33**, 055131.
- Banerjee, S., Krahl, R., Durst, F. & Zenger, Ch. 2007 Presentation of anisotropy properties of turbulence, invariants versus eigenvalue approaches. *Journal of Turbulence* **8**, N32.
- Grossmann, S., Lohse, D. & Sun, C. 2016 High-Reynolds number Taylor-Couette turbulence. *Annu. Rev. Fluid Mech.* **48**, 53–80.
- Hadžiabdić, M., Hanjalić, K. & Mullyadzhano, R. 2013 LES of turbulent flow in a concentric annulus with rotating outer wall. *Int. J. Heat and Fluid Flow* **43**, 74–84.
- Huang, J., Du, Z., Yang, C., Traoré, P. & Wu, J. 2023 Three-dimensional electro-convective flows of dielectric liquids between concentric cylinders. *Int. J. Heat and Fluid Flow* **101**, 1091384.
- Hübner, A.W., Tummers, M.J., Hanjalić, K. & van der Meer, Th.H. 2003 Experiments on a rotating-pipe swirl burner. *Experimental Thermal and Fluid Science* **27**, 481–489.
- Jakirlić, S. & Hanjalić, K. 2002 A new approach to modelling near-wall turbulence energy and stress dissipation. *Journal of Fluid Mechanics* **459**, 139–166.
- Jakirlić, S., Hanjalić, K. & Tropea, C. 2002 Modeling rotating and swirling turbulent flows: A perpetual challenge. *AIAA Journal* **40**(10), 1984–1996.
- Jakirlić, S. & Maduta, R. 2015 Extending the bounds of ‘steady’ RANS closures: Toward an instability-sensitive Reynolds stress model. *Int. J. Heat and Fluid Flow* **51**, 175–194.
- Joksimović, I. & Jakirlić, S. 2023 Eddy-resolving Reynolds-stress modelling of thermal mixing in cross-stream type t-junction configurations. *Applied Thermal Engineering* **235**, 121390.
- Menter, F.R. & Egorov, Y. 2010 The scale-adaptive simulation method for unsteady turbulent flow predictions. part 1: theory and model description. *Flow, Turbulence and Combustion* **85** (1), 113–138.
- Nouri, J.M. & Whitelaw, J.H. 1997 Flow of Newtonian and non-Newtonian fluids in an eccentric annulus with rotation of the inner cylinder. *Int. J. Heat and Fluid Flow* **18**, 236–246.
- Rotta, J.C. 1972 *Turbulente Strömungen. Eine Einführung in die Theorie und ihre Anwendung*. Teubner Verlag Stuttgart.